redin Revista Facultad de Ingeniería, Universidad de Antioquia, No. 81, pp. 9-23, 2016

Experimental framework for laboratory scale microgrids

Marco experimental para microrredes a escala de laboratorio

José Alex Restrepo-Zambrano, José Miguel Ramírez-Scarpetta, Martha Lucia Orozco-Gutiérrez, Jorge Antonio Tenorio-Melo

Grupo de investigación en Control Industrial (GICI), Escuela de Ingeniería Eléctrica y Electrónica, Universidad del Valle. Calle 13 # 100-00. A. A. 25360. Cali, Colombia.

ARTICLE INFO
Received April 14, 2016
Accepted September 16, 2016

KEYWORDS
Microgrid, smart grids, distributed resources

Microrredes, redes inteligentes, fuentes distribuidas

ABSTRACT: This paper presents a proposal for a microgrid test rig for laboratory use. It aims at high flexibility using a modular approach with a common hardware for most of the tasks. The proposed framework for laboratory scale microgrid addresses the requirements for teaching and research. This objective is attained with a reconfigurable power electronics stage, used for test and design of new topologies. The experimental framework also allows testing algorithms at different levels in the hierarchical control structure, while giving access to emulation and simulation of elements commonly found in microgrids and to low-level programming of communication protocols for studying the communications channel. The processing unit in each module, called local controller in the paper, uses a high performance digital signal processor (DSP). This processing unit allows reconfiguration of each module, to assume any of the tasks in the microgrid, i.e. controllable loads, storage, wind, photovoltaic generation, etc. The proposed hardware was tested as a simulator/emulator of the different subsystems. The communications with a microgrid central controller (MCC) is provided with standard embedded processors, capable of implementing the communication protocols suitable for micro-grid environments.

RESUMEN: Este artículo presenta una propuesta de un banco de pruebas de microrredes para uso en laboratorio. El objetivo es proporcionar alta flexibilidad utilizando un enfoque modular con un hardware común para la mayoría de las tareas. El marco experimental propuesto para microrredes a escala de laboratorio proporciona los requisitos para enseñanza e investigación. Esto se logra con una etapa de electrónica de potencia reconfigurable, para pruebas y diseños de nuevas topologías. Permite probar algoritmos en los distintos niveles de la estructura jerárquica de la microrred. Da acceso a la emulación y simulación de elementos encontrados comúnmente en una microrred y a la programación de bajo nivel de los protocolos de comunicación para estudiar el canal de comunicación. La unidad de procesamiento en cada módulo, llamado controlador local, utiliza un procesador digital de señales de alto rendimiento (DSP). Esta unidad de procesamiento permite la reconfiguración de cada módulo para asumir cualquier tarea en la microrred; es decir, como cargas controlables, almacenamiento de energía, generación eólica, generación fotovoltaica, etc. El hardware propuesto se probó operando como emulador de los diferentes subsistemas. Las comunicaciones con un controlador central microrred (MCC) se realizan mediante procesadores integrados estándar, capaces de implementar los protocolos de comunicación adecuados para ambientes de microrred.

1. Introduction

Nowadays, the use of renewable energy such as windmills and photovoltaic arrays, have become an attractive choice to powering residential and commercial buildings, while providing a reasonable carbon footprint at competitive costs [1]. It is expected, for year 2040, an increase of 37% in the world energy demand, with a 33% expected increase in renewable energy [2].

This increase in the use of renewable energy and the outlook of consumption increase in the coming years is driving an increase in the research on new technologies applied to distribution networks, better known as smart grids. In a local level, closer to the final user, the decision-making strategy is more dynamic, and a set of definitions more suited for this level are defined for the so called microgrids. These microgrids are network segments with processing

* Corresponding author: José Alex Restrepo Zambrano
e-mail: restrepo@usb.ve
ISSN 0120-6230
e-ISSN 2422-2844

DOI: 10.17533/udea.redin.n81a02

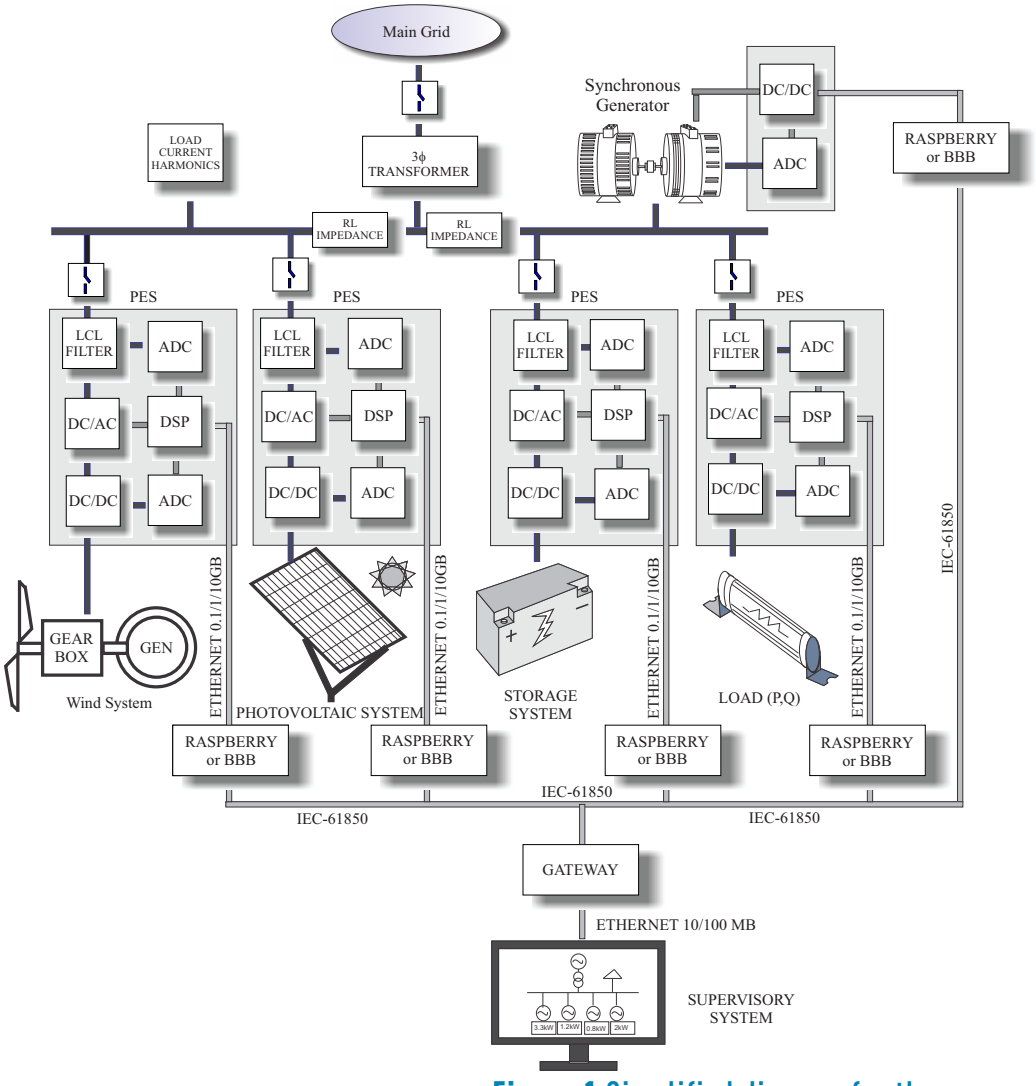

Figure 1 Simplified diagram for the proposed microgrid

power and decision-making capabilities (usually referred as smart), to incorporate renewable energy, distributed storage and able to provide the capability of operating in islanded "isolated" mode. The main objective of these microgrids is to provide the final user with reliable and good quality energy. Figure 1 shows some typical microgrid elements that are included in the proposed microgrid.

The aim of this work is to develop a reconfigurable laboratory for microgrid experiments in teaching and research. The proposed microgrid uses subsystems, of which the ones with controllable semiconductors employ a common customized block for the power electronics front-end, communications and processing unit. This customized common block uses a digital signal processor (DSP) as the local processing unit; a bi-directional active-reactive power (PQ) controlled inverter as its power electronics front-end, and an off-the-shelf microcontroller for the communication tasks. The local processing unit and the communications unit can perform tasks for the associated subsystem, without the need to use the power stage. This capacity allows execution of control code before involving the power stages of the subsystem, useful for real time simulations and emulations in a preliminary stage of the local controller design.

This paper is organized as follows. Section 2 presents previous microgrid laboratory works reported in literature. Section 3 describes the hardware architecture for the proposed test framework for a microgrid scale laboratory; including the power electronic converter and control hardware used to interface the different subsystems (generators, load and storage) composing the microgrid. Section 4 describes each subsystem composing a typical microgrid, such as synchronous generator, energy storage, photovoltaic system, wind generation, and a generic load synthesized with a PQ subsystem. Section 5 describes the architecture defined for controlling the microgrid. Section 6 describes the operation of the microgrid test framework as a simulator, using the processing unit in each subsystem to simulate its behavior and to send to a central control node the corresponding electrical variables of the simulated subsystem. Finally, section 7 summarizes the work presented in this paper.

2. Previous works in microgrid laboratories

The increased penetration of renewable energy is attracting a lot of interest in the use of microgrids and its capability to integrate this energy into the main grid [3], resulting in development of several microgrid laboratory setups around the world. Some of the emblematic developments of these microgrid laboratories are the following.

2.1. Laboratory at CERTS

The basic background of the technology developed at CERTS can be traced back to work on distributed sources using micro-sources [4]. The aim of the CERTS test site is to facilitate development of intelligent autonomous networks [4-6]. The proposed system has three critical components, a static switch, micro-sources and loads. It consists of a group of radial feeders, a single point of connection to the grid (point of common coupling, PCC), feeders with sensitive loads requiring local generation and non critical loads without local generation. The setup includes also some micro-sources, using at one of CERTS sites, as a prime mover a 7.4 liter V-8 modified for gas [7] and the generator is a liquid-cooled permanent magnet machine designed to match the speed-power curve of the prime mover. Each micro-source is coupled to the microgrid through a power conditioning unit, responsible for the power and voltage control for operation in the microgrid. There are four load banks remotely controllable from 0-90 kW and 0-45 kVar. Also, each load bank is equipped with remote faults, ranging from hard faults to high impedance faults (60 kW and 83 kW) [4].

2.2. Microgrid laboratory at the Ohio State University

The test rig proposed by the research group at the Ohio State University uses hardware in the loop based digital simulators as tools to overcome the challenges of a real full power microgrid setup. This real time simulator uses personal computer (PC) based systems with Linux operating system. The system has 4 target machines with a total of 8 processing units, 48 cores, 5 field programmable gate array (FPGA) chips and more than 500 analog and digital I/Os [8] and DOLPHIN PCI boards for high speed interconnection [9]. The proposed system has a number of real time target machines associated to the complexity of the system being simulated. When used in conjunction with a discrete network emulator, the simulation system provides the capability to simulate the communications subsystem and the distributed control. It also allows the identification of key communication elements in the smart grid, such as protocols, bandwidth requirements, cyber security and data management [9, 10]. The system simulated in [9] consists of a local energy storage, a photovoltaic array (PV) and a plug-in hybrid electrical vehicle (PHEV) battery. The breakers in the system are modeled as solid state devices. The simulator is tested for operation in grid connected mode and in islanding mode.

2.3. Laboratory at the Texas A&M University

The work at this laboratory centers on teaching fundamentals of smart grid using simulations and hands on laboratory experiments [11]. Several topics of interest for smart grid are pointed out, including the following: Phasor measurement, digital relaying, protection schemes, impact of PHEVs, uses of smart meters, integration of AC and DC systems, technologies for energy efficiency and green house gas emissions among others. The laboratories are based on modeling and simulation of the system using Matlab/Simulink®. The communications network is modeled using OPNET [12]. This setup allows testing equipment for conformance with standard IEC- 61850-2 and inter-operability tests.

2.4. Laboratory at the CITCEA in the Technical University of Catalonia (CITCEA-UPC)

The microgrid platform at the CITCEA-UPC allows experimental research test in a reduced power scale. It is intended to create a complete microgrid setup where interdisciplinary experiments can be performed, such as: control validation, communication tests, protection analysis and energy management, among others [13]. The laboratory test rig is composed of emulators, using power electronic converters controlling the power flow (active and reactive components) to behave as different elements commonly found in microgrid systems. The microgrid laboratory described in [13] has three different elements, a PV installation, a load and a battery based storage system connected to the main single phase AC grid.

2.5. Laboratory at the CSIRO energy center in Australia

The microgrid laboratory at CSIRO energy center is the result of adapting an existing test site to suit the requirements of the microgrid test setup. The existing facility included: 110 kW of fixed solar photovoltaic, 1 kW of tracking solar photovoltaic, 62 kW of wind turbines, 120 kW of gas micro-turbines, 110 kW of lead-acid battery storage, 110 kW of ultra-battery storage and 500 kW of zinc-bromine flow battery [3]. This existing equipment was upgraded with a gas micro-turbine capable of varying voltage and frequency over a wide range, able to supply up to 30 kVA while producing voltages in the range 200-318 Vrms and frequencies in the range 10 Hz - 60 Hz. A custom built computer controlled load bank provides up to 63 kVA in resistive, inductive and capacitive loads. An instrumentation system collects data at up to 8000 samples per second. A motor is used for experiments in microgrid protection. A control room allows users to perform experiments while having view of the equipment.

2.6. Microgrid test setup at the University of Texas at Arlington

The test rig at the University of Texas at Arlington (UTA), has a total capacity of 11.16 kW comprised of wind turbines, solar panels, proton-membrane fuel cell, diesel generation and marine battery packs acting as main energy storage device [14]. The laboratory setup provides hand-on experience to engineering students. The smart microgrid is composed of three independent microgrids, connected at a point of common coupling (PCC). The single phase utility is also connected at the PCC. The setup is allowed to operate in parallel with the utility grid or in islanding mode. The complete microgrid setup can be operated in different configurations, powering different groups of loads [14].

2.7. Reconfigurable microgrid test bed at Tianjin University

The reconfigurable microgrid test bed at the Tianjin University [15, 16], allows the integration of different energy based resources (renewable and non-renewable). It allows the combined modeling and operation of several types of energy resources, the coordinated control and energy management of the microgrid, studies of interaction between the microgrid and the grid, and studies of different fault schemes.

2.8. Other laboratories around the world

Other microgrid laboratories described in [5, 17-31] deal with distinctive features in their control structure, or as proof of concept with special design characteristics. They make extensive use of commercial systems with difficult to modify firmware needed in teaching and research.

3. Proposed architecture for the laboratory test rig

State of the art microgrids described in the previous section aim at different targets, many unsuitable for teaching and research. The features of interest addressed by the proposed framework are: Communications infrastructure, simple inclusion of new techniques for renewables, study of control issues at different layers in the control hierarchy of the microgrid, among others. The proposed framework is highly reconfigurable, allowing for its simple adaptation according to the needs while providing the possibility to integrate or including commercial units at the highest layer of the control architecture. As mentioned above, it can work as a research test-rig or teaching station for the microgrid elements and also allows including newer subsystems to the test rig or changing existing ones, such as the power stage. These elements are the subject of this work in the next sections. The test rig is required to provide an adaptable framework for power flow control, power electronics testing, energy storage analysis, load shedding, non-islanded (grid connected) and islanded operation and the transition between these states, market management of microgrids and its analysis, study of the communications infrastructure and its reliability, IEC-61850 and IEEE- 1588 protocol analysis, instrumentation and sensors analysis, among others. The architecture of the microgrid test setup is shown in Figure 1. It uses a reconfigurable power electronics converter to interface with the main grid different subsystems composing the microgrid, such as photovoltaic (PV), wind, storage and load.

The modules part of the microgrid subsystem share a similar power electronics stage to interface with the grid at a point of common coupling (PCC). This power converter is described below, together with each subsystem in the proposed microgrid.

3.1. Power electronics stage

Several subsystems connect to the microgrid through a power electronic converter. There are different kinds of topologies that can be used to interface the microgrid devices to the grid. The test rig proposed in this work is required to be flexible enough to accommodate different power converters. There are many topologies available at the moment, some of these topologies for the converters are described in literature, and the ones used in this setup are described below.

1) Standard three phase full bridge topology: This is the simplest and widely used topology for general applications in three phase systems [32]. Figure 2(a) shows the typical three phase full bridge topology. For some systems in the microgrid, such as the PV, a transformerless connection to the grid imposes severe restrictions that make unfeasible its use [32]. Current technology on insulated gate bipolar transistors allows using these converters with a 6.5 kV maximum voltage in the DC link for connecting directly to the grid [33]. In this work only the classical Three-Phase Voltage Source Inverter, shown in Figure 2(a) is considered for the front end power converters.

2) Multilevel converters: There is a plethora of topologies, mainly due to the number of levels and modulation strategies, related to multilevel converters. Its complexity is compensated with the advantages obtained by using the additional switching states, such as fault tolerant capabilities and extended voltage range of operation. Figure 2(b) shows the classical Three-Phase Neutral-Point-Clamped Voltage Source Inverter [34] that can be implemented with the proposed hardware.

3) Z voltage source inverters: Z voltage source inverters (ZVSI) [35-37] and quasi-ZVSI [38, 39] are modern topologies for the power stage aiming at providing DC-AC conversion while allowing DC-DC boost of the DC supply. These topologies also allow simultaneous switching of upper and lower devices, otherwise forbidden in conventional DC-AC or AC-DC voltage source converters. Figure 2(c) [35] shows some impedance in the path between

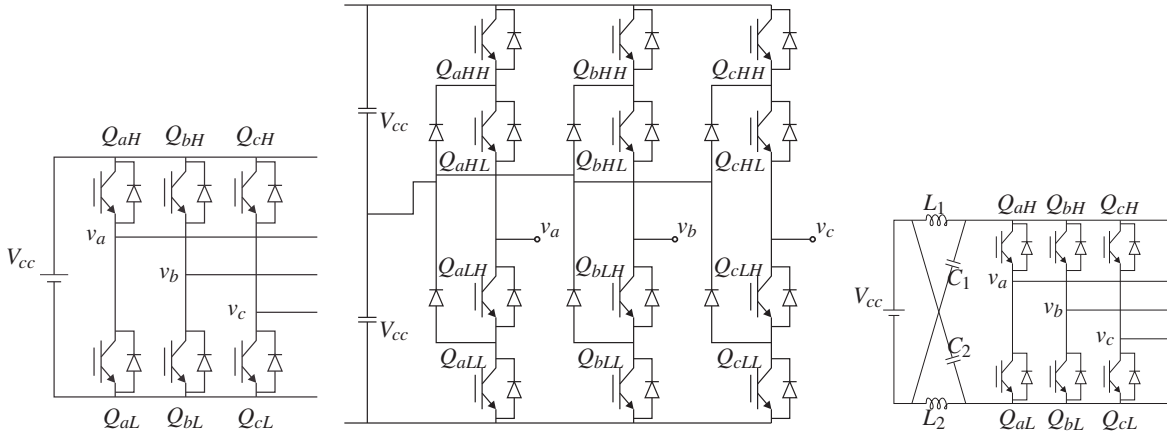

(a) Three phase full bridge topology

(b) Three phase neutral point clamped voltage source inverter.

(c) Three phase Z-voltage source inverter.

Figure 2 Power electronics stage used by the microgrid subsystems

the DC supply and the power devices of the converter that allows for the simultaneous switching of the upper and lower devices in the same phase (shoot-through state). This also results in an increase of the fault tolerance capability of this kind of converters. A promising topology is the quasi-switched boost inverters [40], but battery storage capability needs to be investigated.

3.2. Local controller

There are several levels of control in the system for proper operation of the microgrid, and several strategies to achieve effective regulation of power flow at the point of common coupling of each distributed energy resource (DER). The innermost control, and the fastest in the system, corresponds to local controllers. A local controller in the proposed system has the capability to operate on a group of power converters that are in physical proximity to each other, as long as the processing requirements are properly bounded. Figure 3 shows the structure of the processing and interface cards employed by the local controllers.

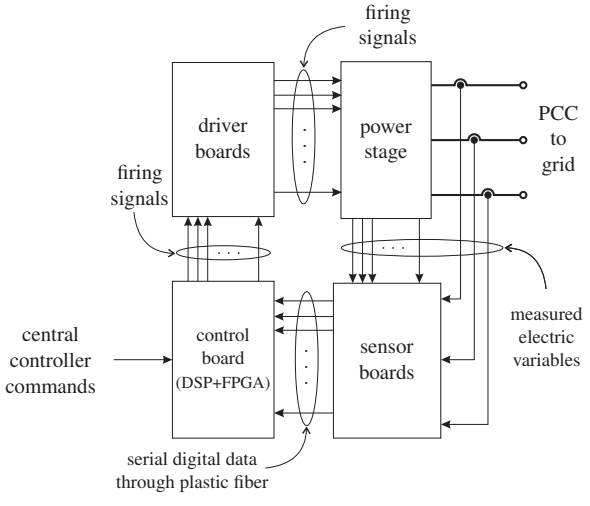

Figure 3 Local controller's hardware block diagram

1) DSP based control unit: The main processing unit uses an Analog Devices DSP, paired to an FPGA based interface board. Programming of the DSP can be done from a PC through an USB connection, using C, C++ or assembly languages. After downloading the code, the system can operate autonomously, and optionally can receive operating settings from a central controller through an embedded card described below. The DSP is housed in an evaluation board for the Analog Devices ADSP-21369 (DSP-21369 EZ-KIT Lite ®) [41], capable of a peak 2.4 GFLOPS while running at 400 MHz.

2) FPGA board: The control signals exchanged with the power stage are routed through an interface board housing an FPGA. The FPGA board has three 3-phase pulse width modulation (PWM) modules, control logic for serial communication to two sensor boards and logic for measuring time interval (used to measure speed), and interruption generation for synchronizing the control loops in the local controllers.

3) Sensor board: The PWM carrier module synchronizes the parallel acquisition in all the conversion channels. The analog to digital converter has 16-bits resolution and a conversion time of 4 μs, but data is available to the processing unit in about 16 μs after the start of the PWM carrier sweep. Once the acquisitions are available, the FPGA triggers an interrupt to the DSP to signal the start of the control cycle. This operation is executed without intervention of the user, and is hardwired in the FPGA.

3.3. Communications and time stamping

The local controller connects to the Ethernet link through either a Raspberry Pi 2 or a Beaglebone Black (RPI/BBB) board, as shown in Figure 1. On the other hand, the RPI/BBB board connects to the DSP through a serial peripheral interface (SPI) link and allows data exchange between the

DSP board and the outside world throughout Ethernet. Transmission of data requires a precise time stamp, in compliance with standard IEEE-1588 [42]. The RPI/BBB board will provide the precision time stamping using a global positioning system (GPS) connected to one of its peripheral ports. Communication between the RPI/BBB board and the MCC follows standard IEC-61850 [43] for interconnecting DERs. Thanks to its capacity to interface devices operating under different data protocols, standard IEC-61850 enables the integration of protection, control, measurement and monitoring tasks into the microgrid. The central station shown in Figure 1 uses the commercial supervisory system ETAP in which a human-machine interface allows an operator to monitor and command variables and equipments involved in the microgrid operation. At the same time, this station executes the highest level of control, regulating the energy flow to the DERs. A gateway device interfaces the Ethernet link to the ETAP software, allowing data exchange under the IEC-61850 Ethernet protocol.

4. Microgrid elements

All the subsystems making up the microgrid were first individually simulated using Matlab/Simulink® for a first approach in selecting proper working conditions. Afterwards, a C language description of the subsystem, and its local controller, provides a representation with a behavior that is a step closer to the subsystem's hardware. This C language description of the subsystem runs on the experimental test rig, and the control actions of the local controller go to the state equations model of the subsystem. This approach allows at a later design stage to send the control actions to the real hardware. Figure 1 shows a simplified diagram of an initial prototype for the microgrid, as the structure of this microgrid will allow its future grow and modification.

4.1. Controllable and fixed loads (PQ subsystem)

The PQ subsystem allows the simulation of variable loads, with different active and reactive content. This subsystem will present also the possibility to emulate a distributed source, or act as an active filter. The capabilities of this subsystem are possible thanks to the use of direct power control with arbitrary active and reactive commands [44]. Figure 4 shows a diagram of voltage source converter operating with an optimal space vector selector for direct power control.

Direct power control is based on the instantaneous apparent power [44, 45]. Using the current and voltage space vectors definitions the instantaneous apparent power results in (1),

$$\vec{s} = \vec{v}_s . \vec{i}_s^{\,*} = \left(v_{s\alpha} + jv_{s\beta}\right).\left(i_{s\alpha} + ji_{s\beta}\right)^{*} = p + jq. \tag{1}$$

From Figure 4, for simple coupling inductances (L_s–R_s), the subsystem can be modeled as described by (2),

$$\vec{v}_s = \vec{v}_r + R_s \vec{i}_s + L_s \frac{d\vec{i}_s}{dt}\ , \tag{2}$$

where $\vec{v}_s$, $\vec{v}_r$ and $\vec{i}_s$ are the space vectors for the grid voltage, the inverter voltage and the PQ subsystem's current. A discrete time version of this equation can be obtained by applying a first order approximation, such as the approximation in (3) for the system current [44],

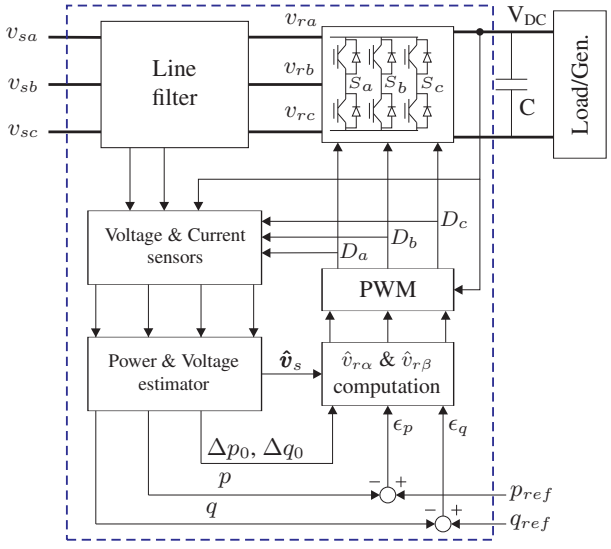

Figure 4 Block diagram of the optimum direct power control acting as a PQ subsystem (PQ front-end)

$$\hat{\vec{i}}_s\left(k+1\right) = \vec{i}_s\left(k\right) + \Delta\hat{\vec{i}}_s\left(k\right) \tag{3}$$

After some mathematical manipulations, described in [44], for a given reference in active and reactive power, p_{ref} and q_{ref}, the required value in the following sampling period for the change in apparent power and its errors are given by (4) and (5),

$$\Delta\vec{s}\left(k\right) = \Delta\vec{s}_0\left(k\right) - \frac{T_s}{\hat{L}_s}\left[\hat{\vec{v}}_s\left(k+1\right).\hat{\vec{v}}_r\left(k\right)^{*}\right] \tag{4}$$

$$\vec{\varepsilon}_s\left(k\right) = p_{ref} - Re\left\{\vec{s}\left(k\right)\right\} + jq_{ref} - Im\left\{\vec{s}\left(k\right)\right\} \tag{5}$$

$\hat{L}_s$ is the estimated coupling inductance and T_s is the

sampling period. Finally, the absolute optimum voltage required to attain the commanded active and reactive power is given by (6),

$$\hat{\vec{v}}_r(k)=\vec{v}_{r\alpha}(k)+j\hat{v}_{r\beta}(k)=\frac{\hat{L_s}}{T_s}\left[\frac{\Delta\vec{s}_0(k)-\vec{\varepsilon}_s(k)}{\vec{v}_s(k).e^{j\omega T_s}}\right]^* \quad (6)$$

4.2. Synchronous generator

The synchronous generator provides support energy to the microgrid during periods of time of high demand. In general, the cost of this energy is expensive due to the cost of the equipment and the fuel required by the primary mover. The proposed microgrid setup uses a synchronous generator (Figure 5(a)) already present in the research laboratory and adapted for operation in the microgrid. The synchronous generator parameters are enumerated in Table 1 [46] and the synchronous generator sub-system is simulated using the dynamic Eqs. (7-10) [47].

$$v_{sd}=R_s i_{sd}+L_d\frac{di_{sd}}{dt}-\omega_r L_q i_{sq}+L_{df}\frac{di_f}{dt} \quad (7)$$

$$v_{sq}=R_s i_{sq}+L_q\frac{di_{sq}}{dt}+\omega_r L_d i_{sd}+\omega_r L_{df} i_f \quad (8)$$

$$v_f=R_f i_f+L_f\frac{di_f}{dt}+L_{df}\frac{di_{sd}}{dt} \quad (9)$$

$$J\frac{d\omega_r}{dt}+\rho\omega_r-\tau_m=\frac{P}{2}\left[\left(L_d-L_q\right)i_{sd}i_{sq}+L_{df}i_{sq}i_f\right] \quad (10)$$

where $v_{s\{d,q\}}$ and $i_{s\{d,q\}}$ are the direct and quadrature stator voltage and currents respectively, i_f is the field current, J is the inertia, ρ is a damping coefficient, τ_m is the mechanical load, ω_r is the angular electrical speed, and the machines parameters are P, R_s, R_f, L_d, L_q, L_{df}, L_f.

Additionally to the field winding, there are damper windings in the rotor in the same axis as the field winding and 90° ahead. These damper windings will appear as additional terms and equations in the machine model [46, 48], but they are neglected in the simulations of the synchronous generator. This dynamic model allows the simulation of transient events in the machine's supply or in its mechanical load. Figure 5(b) shows the Simulink diagram used to verify the operation of the generator model.

Table 1 Synchronous generator parameters

$r_s = 382\ m\Omega$	$L_{ls} = 1.12\ mH$	$L_{mq} = 24.9\ mH$	$r_{kd1} = 140\ \Omega$	$L_{lkd1} = 9.87\ mH$
$r_{kq1} = 5.07\ \Omega$	$r_{kd2} = 1.19\ k\Omega$	$L_{lkd2} = 4.91\ mH$	$r_{kq2} = 1.06\ \Omega$	$r_{kd3} = 1.58\ \Omega$
$L_{lkd3} = 4.52\ mH$	$r_{kq3} = 447\ mH$	$r_{fd} = 112\ mH$	$L_{lfd} = 1.53\ mH$	$\frac{N_s}{N_{fd}} = 0.0269$
$L_{md} = 39.3\ mH$	$L_{lkq1} = 4.21\ mH$	$L_{lkq2} = 3.5\ mH$	$L_{lkq3} = 26.2\ mH$	4 poles

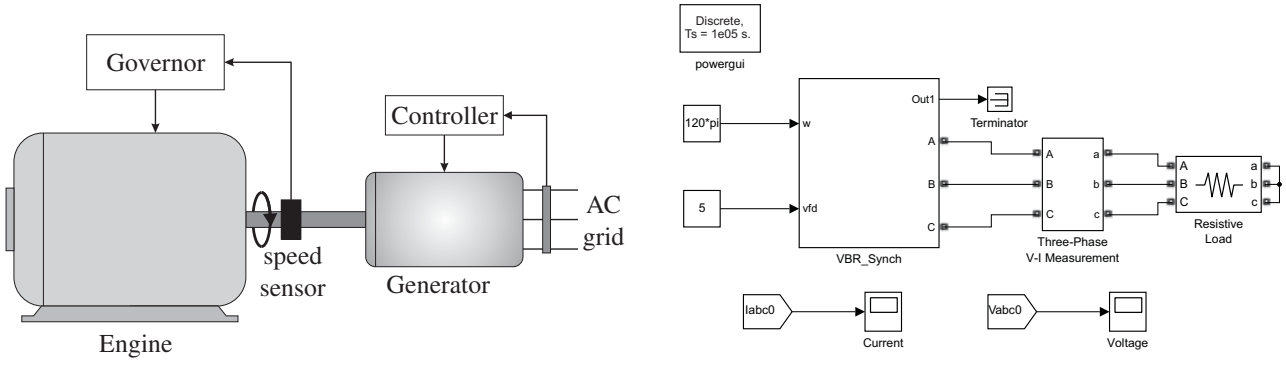

(a) Operation of the synchronous generator coupled to the microgrid.

(b) Matlab model of the synchronous generator.

Figure 5 Synchronous generator subsystem

The primary mover is simulated using the speed drop versus torque function (11), in the τ,ω plane. This results in a drop in frequency with an increase in load that can be compensated with the machine's governor.

$$\omega_m = \omega_0 - \frac{\Delta\omega}{\Delta\tau}\tau_m, \tag{11}$$

where Δω is the change in speed of the primary mover due to a corresponding $\Delta\tau$ in the primary mover shaft's load torque.

4.3. Storage

In microgrids, the generation from renewables is dependent on weather conditions, so it is not controllable. Also, apart from normal load changes, microgrids may have power changes near to the generation capacity, which can lead to a high imbalances and instability. An objective of the microgrid is to obtain the correct balance between generation and demand, and that requires an energy storage system [49].

The microgrid proposed in this work uses a centralized energy storage system [49], shown schematically in Figure 1, where a battery bank is connected to the microgrid's central node. The energy storage system is composed of storage elements, power electronic interface and control strategies. The storage elements are four 12 V lead-acid batteries. The power electronic interface is bidirectional for charging and discharging the storage element and further adjusts the DC level to the inverter side, as shown in Figure 6.

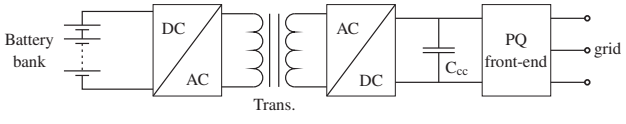

Figure 6 Power electronic interface with high frequency transformer [49]

The control strategies, besides to supply power and support the voltage regulation, should avoid battery overload and over-discharge with an adequate control of the state of charge (SOC) describing the percentage of remaining capacity. The charge and discharge cycle has an effect on the life of the battery. A new fully charged battery has 100% SOC. In an aged battery the internal resistance increases due to active material isolation; the SOC of a battery is the product of the current and the duration of the discharge and can be determined from the previous capacity history and the capacity charged or discharged. Eq. (12) shows the SOC as a function of time [50],

$$SOC(t) = SOC(t_0) - \frac{1}{AHC}\int_{t_0}^{t} i(\tau)\,d\tau \tag{12}$$

where *SOC(t0)* is the previous SOC of the battery, AHC is the ampere hour capacity of the fully charged battery, and $i(\tau)$ is the discharge current.

4.4. Photovoltaic subsystem

A real photovoltaic (PV) generator subsystem will be integrated to the microgrid. Figure 7(a) shows a general diagram of the existing PV field, composed by sixteen PV panels, capable of providing 1.9 kW. These panels are connected in a series-parallel configuration; it provides a maximum output voltage of 354.8 V. Thus, a DC/DC boost converter is required to increase the DC bus voltage level. At the same time, a maximum power point tracking algorithm is used to extract the maximum power from the PV field. The voltage, current, temperature and irradiance level of the PV field is obtained by a digital electronic microprocessor based system. The PV system is able to change dynamically the connection among the PV panels, which is a strategy to increase the efficiency when the panels are subjected to mismatching conditions [51]. In this strategy, the panels are interconnected through a switching matrix, which is an electronic circuit that uses switches to connect the panels in series or parallel. An optimal reconfiguration algorithm determines the panels' interconnection, such

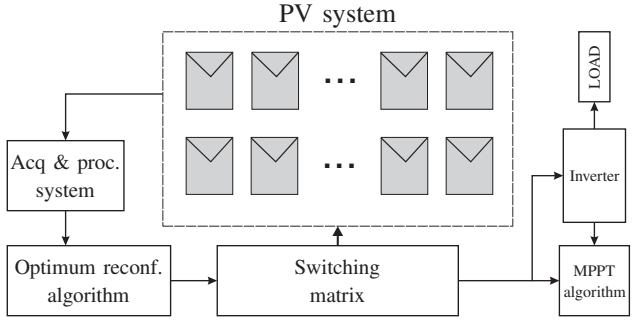

(a) Block Diagram of the PV system.

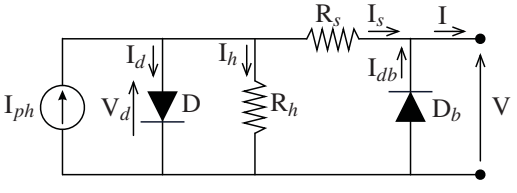

(b) Single-diode model of a PV panel.

Figure 7 PV subsystem models

that the system's constraints are satisfied. Each PV panel is represented by the circuit model shown in Figure 7(b). This model includes a photocurrent generator, the diode D represents the nonlinearity, R_s and R_h represent the losses in the PV panel. A bypass diode is connected in parallel to each panel, which avoids losses in a string and protects from damage mismatched PV cells [52].

In [53] the Lambert W-function was proposed for achieving an explicit expression of the output current and of its derivative, which are given in (13) and (14). In [54] a computationally efficient approach to the modeling of a photovoltaic array is proposed, which is able to simulate strings subjected to mismatching conditions. That proposed solution is based on an explicit symbolic calculation of the inverse of the Jacobian matrix to solve the non linear system of equations describing the photovoltaic array.

$$I=\frac{R_h\left(I_{ph}+I_{sat,d}\right)-V}{R_h+R_s}+I_{sat,db}\left(e^{-V/V_{t,db}}-1\right)-\frac{V_{t,d}}{R_s}LambertW\left(\theta\right) \tag{13}$$

$$\frac{dI}{dV}=-\frac{1}{R_h+R_s}-\frac{I_{sat,db}}{V_{t,db}}e^{-V/V_{t,db}}-\frac{R_h}{R_s\left(R_h+R_s\right)}LambertW\left(\theta\right) \tag{14}$$

The expression for θ is shown in (15).

$$\theta=\frac{\left(R_s\,||\,R_h\right)I_{sat,d}e^{\left(R_sR_h\left(I_{ph}+I_{sat,d}\right)+\left(R_hV/V_{t,d}\right)\left(R_h+R_s\right)\right)}}{V_{t,d}} \tag{15}$$

4.5. Wind generator

The wind generator subsystem for this micro grid will be simulated at the DC bus voltage level, as a compromise between the real system and an emulation of the mechanical system. Figure 8(a) shows a diagram of the wind turbine nacelle, and Figure 8(b) shows the block diagram of a typical wind turbine employing a synchronous generator.

The power taken from the wind depends on the power coefficient C_p, that depends on the tip-speed ratio λ as defined in (16) [55]:

$$\lambda=\frac{\text{blade tip speed}}{\text{wind speed}} \tag{16}$$

The value for the power coefficient can be extracted from data provided by the wind generator manufacturers, or from mathematical models fitting that data [55, 56]. The simulator in the wind generator subsystem uses Eq. (17) for the power coefficient and Eq. (18) for the equivalent wind power injected to the DC bus [57].

$$C_p=c_1\left(c_2-c_3\beta-c_4\beta^x-c_5\right)e^{c_6\left(\lambda,\beta\right)} \tag{17}$$

$$P_w=\frac{1}{2}\rho A_TV_T\left(V^2-V_s^2\right)=\frac{1}{2}\rho A_TV_TC_p=P_vC_p \tag{18}$$

where A_T is the area of the disc formed by the turbine's blades, V_T is the wind speed in the turbine and V_s is the wind speed after the turbine's blades, P_v is the wind power and C_p is the power coefficient described previously.

This power (*Pw*) will be the set point for the active power of a direct power controlled inverter [44] that will inject into the grid the simulated wind power. Figure 9(a) shows the set of wind power curves used by the wind subsystem emulator, for C_p as a function of the tip speed ratio λ and the pitch angle β, using the following coefficients in (17):

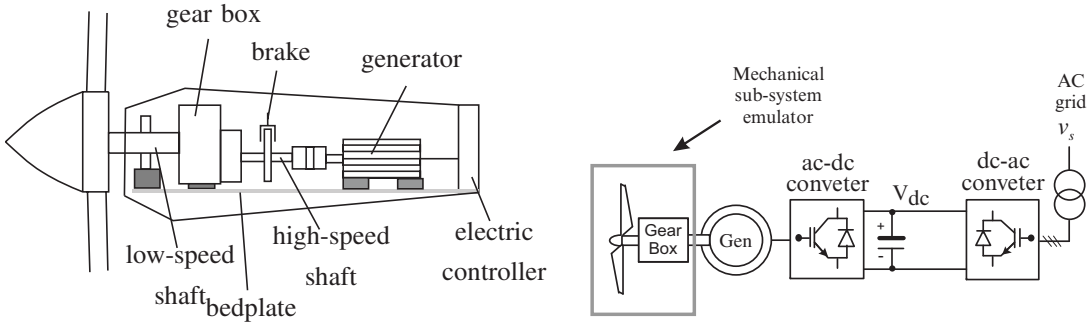

(a) Diagram of the wind-turbine's nacelle.

(b) Block diagram of the synchronous generator based wind turbine.

Figure 8 Diagram of the wind-turbine's nacelle and its interface to the grid

c_1=0.5 c_2=116/λ_i c_3=0.4 c_4=0 c_5=5 c_6=21/λ_i with λ_i as shown in (19),

$$\lambda_i = \left[\frac{1}{\lambda + 0.08\beta} - \frac{0.035}{\beta^3 + 1} \right]^{-1} \quad (19)$$

The wind generation subsystem's emulation uses wind speed information, such as the presented in Figure 9(b) [58], together with (18), to feed into the grid the corresponding wind active power. This active power injection is done using a power electronics front end similar to the one described in section 4-A.

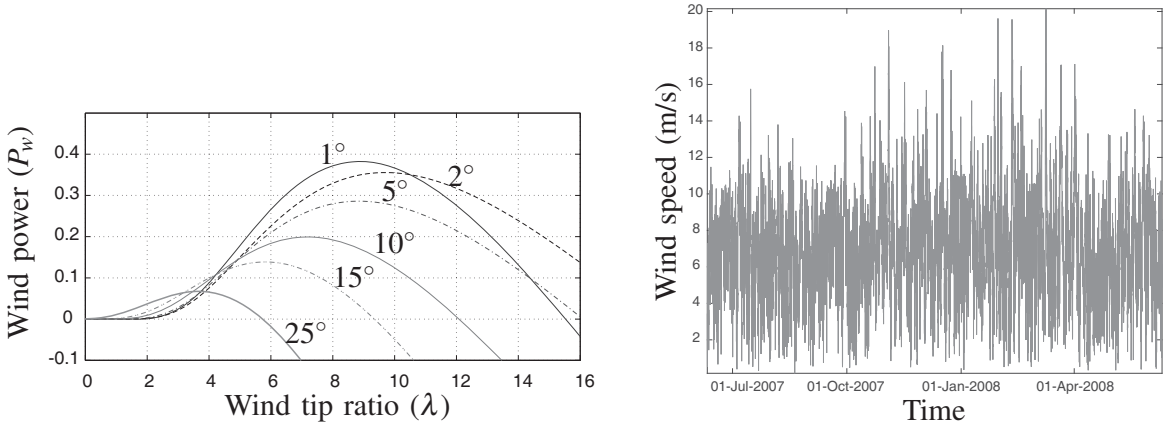

(a) Wind power versus wind tip ratio (λ) for different blade attack angles.

(b) Simulated wind data.

Figure 9 Power-λ curves and simulated wind data for the wind subsystem

5. Control of the microgrid

In a microgrid, dynamic and static performance, together with some economic aspects, are regulated through a hierarchical structure [59]. This structure is composed of levels which follow the standard IEC/SAC-62264, shown in Figure 10.

Zero level consists of the control loops of outputs current and voltage from the inverter. When the microgrid is not connected to the main grid through the PCC (isolated mode), electronic power converters connected to the microgrid operate as voltage source inverter to control the voltage and frequency of the microgrid [60]. When the microgrid is connected to the main grid, the inverters share active or reactive power operating as current source inverters [61, 62]. The role of these power electronics converters is to regulate the power flow between electric power generators (renewable energy sources and electric storage systems) and the grid.

First level, (known as primary control) generates the reference value for the inner control loop (frequency and amplitude of the voltage). This control could have a quick response (in the order of milliseconds), so that a lower response time improves power system stability. The primary control is used to share load between distributed generation (DG) units and the electric storage elements. The contribution of active power can be adjusted in line with the availability of energy from each DG unit and depending on the batteries' state of charge [63]. These controls are classified among those dependent on communications systems as: The central controller, master –slave control, instantaneous (average) current sharing, peak-value based current sharing, circular chain control (3C), among others [64, 65]. Also, as not dependent on communications systems as: droop control, virtual output impedance control, virtual frame transformation method, adaptive voltage droop control, signal injection method, etc. [64, 65].

Second level, (know as secondary control) works to compensate for voltage and frequency errors and to regulate the value in the operational limits of the microgrid (see IEE1547 2003 and 2011, IEC 62257, IEEE 412.2 and C84.1-1995 standards). The response of this control is slower than the primary control (in the order of minutes). At this level of control, electrical storage systems play an important role in the short term compensation of voltage and frequency deviations [49, 66]. Compensation voltage and frequency can be performed using a centralized control [67] or distributed control [68].

Third level, (know as tertiary control) manages the power flow and interface between the microgrid and the main grid. Power flow control, re-synchronization between microgrid and main grid, adjustments of voltage and frequency in both modes, optimal and efficient energy dispatch comprise the key principles of the microgrid control structure [69, 70]. Fourth level corresponds to planning and logistics on a daily basis dispatch.

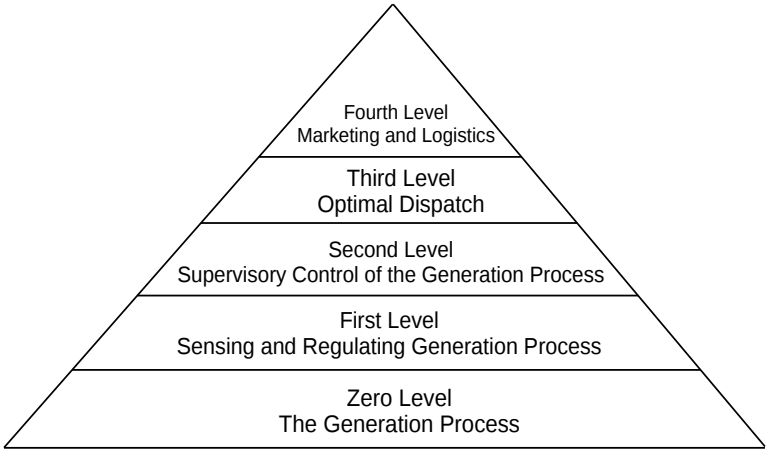

Figure 10 Hierarchical control structure, standard IEC / SAC 62264

6. Operation of the subsystems as simulators

For testing the Ethernet link between the MCC and the local controller, a PC runs the client software programmed in C language. The personal computer is a DELL XPS-8700 running Linux Fedora 22. In the local controller, the server runs on an embedded board connected to the DSP through an SPI port using a 1MHz clock. The PC and the embedded board connect through a 200Mbps Ethernet switch connected to a 150 Mbps router. Both the PC and the embedded processor use a 10/100Mbps Ethernet port. For these tests the router connects only the MCC with the embedded board.

The experimental test-rig runs a simulation of the microgrid described in Figure 1 for testing the communication performance for three different embedded boards connected to the local controller DSP. The Ethernet communications link is tested using an echo with user datagram protocol (UDP) between a client program running in the PC and a server program running in the embedded board. The three different embedded boards used for the test have the following characteristics.

1. Raspberry PI 2 running a Linux operating system with raspberrypi 4.1.15-rt17+ kernel.
2. Beaglebone Black running Linux with the 3.8.13-bone79.
3. TI TM4C1294 embedded board without operating system.

Table 2 shows the execution time for an echo test between a client system and the DSP board for the different embedded servers described above. Figure 11 shows the Simulink® diagram for the Matlab/Simulink communication tests. Figure 12 shows the SPI transaction between the Raspberry server and the DSP, after successive data requests from a client in the MCC. The gaps between the SPI packets corresponds to the time transit in the Ethernet channel connecting the Raspberry board with the MCC. For the test shown in Figure 12 the time elapsed between a consecutive data transfer (time between markers A and B) is 1.65535 ms.

Table 2 Execution time for echoing five single precision floating point numbers between a client system and the dsp board connected to different embedded servers

Connection	Client	Server	Max. (ms)	Min. (ms)	Ave. (ms)	Std. deviation (μs)	Programming complexity
Wired	C Language	Raspberry PI 2	8.33418	1.45430	1.72572	332.35	Medium
		Beaglebone Black	7.71340	0.95280	1.03465	163.02	
		TI TM4C1294	0.71784	0.61356	0.66460	21.05	Very high
	Matlab Simulink	Raspberry PI 2	20.77781	2.28568	10.2716	1001.35	Low
		Beaglebone Black	57.44802	1.56978	10.2903	1207.64	
		TI TM4C1294	21.64216	0.70333	10.1339	1142.15	High
Wireless	C Language	Raspberry PI 2	21.92191	2.13291	2.75612	853.93	Medium
		Beaglebone Black	19.57067	1.89546	2.61451	1041.31	
		TI TM4C1294	13.07593	1.36426	1.92075	716.85	Very High
	Matlab Simulink	Raspberry PI 2	44.61420	2.68577	10.4113	1750.84	Low
		Beaglebone Black	23.06999	2.86914	10.3418	1428.23	
		TI TM4C1294	41.04928	1.93988	10.3438	1291.59	High

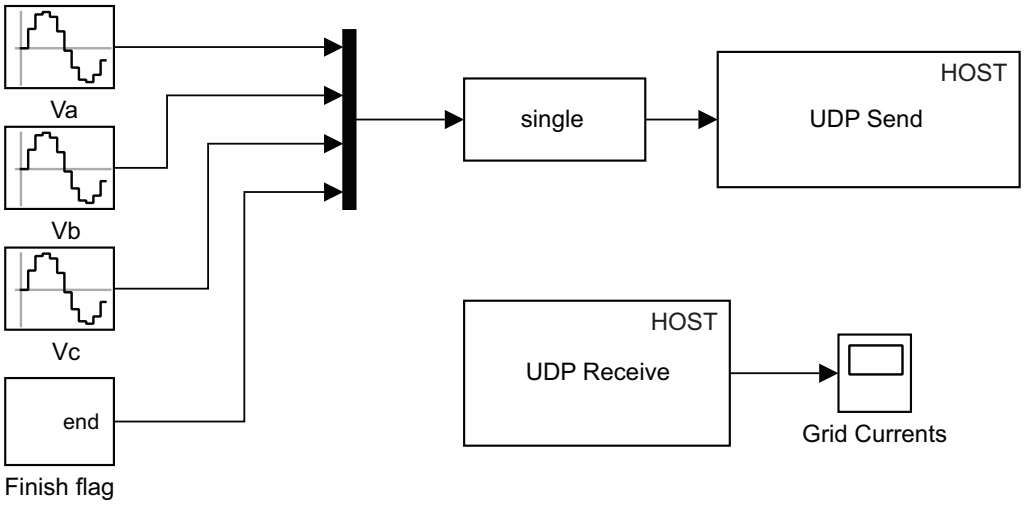

Figure 11 Simulink model for the microgrid central controller

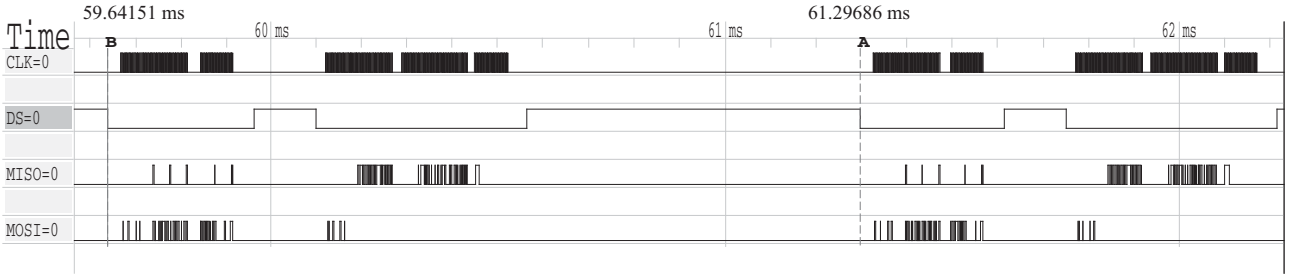

Figure 12 SPI transaction for wired communication between a client in the PC side, using C language, and a Raspberry server local controller side

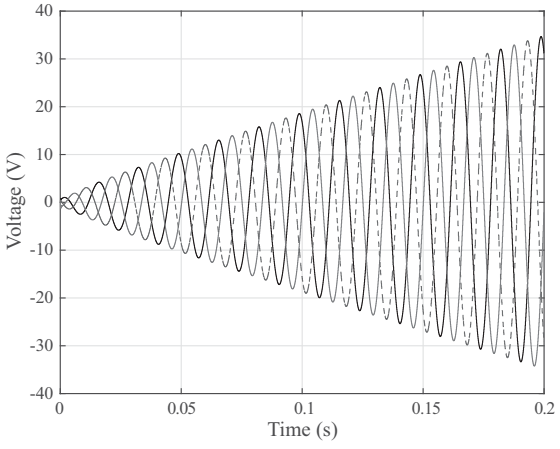

(a) Simulated synchronous generator stator voltages during start-up.

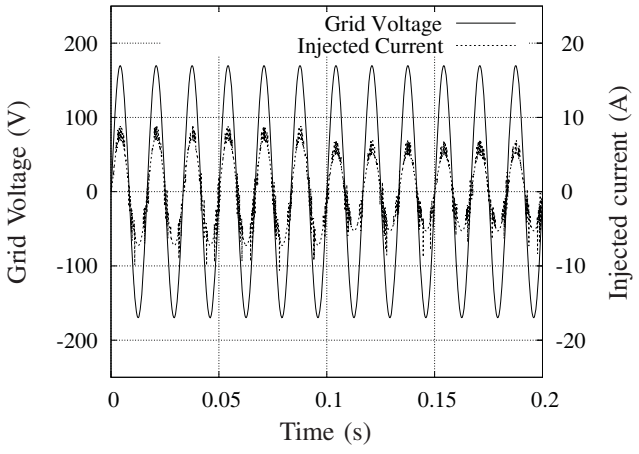

(b) Simulated wind generator injected current during a change in its set-point.

Figure 13 Simulation of the synchronous and wind generators

6.1. Simulation of the synchronous generator using the processor in the local controller

Figure 13(a) shows the simulated voltages for a synchronous generator, implemented in C-language and using (7)-(11). For the simulation the generator runs at constant speed and is loaded with a three phase resistive bank.

6.2. Simulation of the wind generator using the processor in the local controller

Figure 13(b) shows the simulated grid voltage and current injected to the grid in phase 'a' from the wind subsystem using (16)-(19). The changes in the set-point for the amount of current drawn from the converter is very slow compared to the signals dynamics, and Figure 13(b) shows at t = 0.1s a change in this set point.

7. Conclusion

Section 2 of this article has presented a list of works related to microgrid laboratory implementations, published previously by several authors. This gives a background for the microgrid laboratory developed in this work. Then, a comprehensive description of the hardware architecture for a laboratory scale microgrid provides information of the inner working of several customized and flexible power electronics hardware. The experimental framework for microgrids proposed in this work, addresses the main requirements for teaching and research. First, it has a reconfigurable power electronics stage. Second, it allows control strategies at all hierarchical levels. Third, it allows to emulate/simulate various sources of generation and load types. Finally, the experimental framework opens the possibility of adjusting the low level communication protocols.

As an example, this hardware integrates wind and photovoltaic power generation, an adjustable load, an energy storage with batteries and a low power synchronous generator for critical loads, all this coordinated by standardized communication protocols and control hierarchies. The proposed test bed laboratory allows centralized survey, real-time simulation and implementation of controllers at different hierarchical levels.

Each subsystem in the microgrid working as a simulator has allowed testing of the microgrid controllers and communication protocols. Future work is under way for running the power electronic stages feeding or taking power to or from the microgrid.

The customized cards used in each subsystem provide more insight into different microgrid elements. This provides the possibility to alter any stage of the design, allowing the use of new parts and testing other hardware topologies and control strategies.

8. Acknowledgments

The authors gratefully acknowledge the support of Universidad del Valle and Colciencias under Research Project #FP-501-2014.

9. References

1. Varun, I. Bhat, and R. Prakash, "LCA of renewable energy for electricity generation systems—a review," *Renewable and Sustainable Energy Reviews*, vol. 13, no. 5, pp. 1067-1073, 2009.
2. International Energy Agency (IEA), *World Energy Outlook 2014 FACTSHEET*. [Online]. Available: http://www.worldenergyoutlook.org/media/weowebsite/2014/WEO2014FactSheets.pdf. Accessed on: Mar. 12, 2016.
3. D. Cornforth, A. Berry, and T. Moore, "Building a microgrid laboratory," in *IEEE 8th International Conference on Power Electronics and ECCE Asia* (ICPE & ECCE), Jeju, South Korea, 2011, pp. 2035–2042.
4. R. Lasseter *et al.*, "Certs microgrid laboratory test bed," *IEEE Transactions on Power Delivery*, vol. 26, no. 1, pp. 325–332, 2011.
5. S. Krishnamurthy, T. Jahns, and R. Lasseter, "The operation of diesel gensets in a certs microgrid," in *IEEE Power and Energy Society General Meeting - Conversion and Delivery of Electrical Energy in the 21st Century*, Pittsburgh, USA, 2008, pp. 1–8.
6. R. Lasseter and P. Paigi, "Microgrid: a conceptual solution," in *IEEE 35th Annual Power Electronics Specialists Conference* (PESC), Aachen, Germany, 2004, pp. 4285–4290.
7. R. Panora, J. Gehret, and P. Piagi, "Design and testing of an inverter-based combined heat and power module for special application in a microgrid," in *IEEE Power Engineering Society General Meeting*, Tampa, USA, 2007, pp. 1–8.
8. Opal-RT Technologies, *Opal-RT Technologies*. [Online]. Available: http://www.opalrt.com. Accessed on: Mar. 14, 2016.
9. F. Guo *et al.*, "Real time simulation for the study on smart grid," in *IEEE Energy Conversion Congress and Exposition* (ECCE), Phoenix, USA, 2011, pp. 1013–1018.
10. P. Parikh, M. Kanabar, and T. Sidhu, "Opportunities and challenges of wireless communication technologies for smart grid applications," in *IEEE Power and Energy Soc. General Meeting*, Minneapolis, USA, 2010, pp. 1–7.
11. M. Kezunovic, "Teaching the smart grid fundamentals using modeling, simulation, and hands-on laboratory experiments," in *IEEE Power and Energy Society General Meeting*, Minneapolis, USA, 2010, pp. 1–6.
12. OPNET Technologies, Inc., *OPNET Modeler, OPNET Technologies*. [Online]. Available: http://www.opnet.com. Accessed on: Mar. 14, 2016.
13. E. Prieto, M. Cheah, R. Villafafila, O. Gomis, and A. Junyent, "Development of a laboratory platform for testing new solutions to integrate renewable energy sources in power systems," in *15th European Conference on Power Electronics and Applications* (EPE), Lille, France, 2013, pp. 1–10.

14. M. Liu, Z. Ding, F. Quilumba, W. J. Lee, and D. Wetz, "Using a microgrid test bed to evaluate the strategies for seamless renewable energy integration," in *IEEE/IAS 50th Industrial & Commercial Power Systems Technical Conference* (I&CPS), Fort Worth, USA, 2014, pp. 1–9.
15. Y. Che, Z. Yang, and K. Cheng, "Construction, operation and control of a laboratory-scale microgrid," in *3rd Int. Conference on Power Electronics Systems and Applications* (PESA), Hong Kong, China, 2009, pp. 1–5.
16. C. Wang *et al.*, "A highly integrated and reconfigurable microgrid testbed with hybrid distributed energy sources," *IEEE Transactions on Smart Grid*, vol. 7, no. 1, pp. 451–459, 2016.
17. M. Rasheduzzaman, B. Chowdhury, and S. Bhaskara, "Converting an old machines lab into a functioning power network with a microgrid for education," *IEEE Trans. on Power Systems*, vol. 29, no. 4, pp. 1952–1962, 2014.
18. M. Barnes *et al.*, "Microgrid laboratory facilities," in *International Conference on Future Power Systems*, Amsterdam, Netherlands, 2005, pp. 1–6.
19. J. Weimer *et al.*, "A virtual laboratory for micro-grid information and communication infrastructures," in *3rd IEEE PES International Conference and Exhibition on Innovative Smart Grid Technologies* (ISGT Europe), Berlin, Germany, 2012, pp. 1–6.
20. F. Katiraei, C. Abbey, S. Tang, and M. Gauthier, "Planned islanding on rural feeders 2014; utility perspective," in *IEEE Power and Energy Society General Meeting - Conversion and Delivery of Electrical Energy in the 21st Century*, Pittsburgh, USA, 2008, pp. 1–6.
21. N. Lidula and A. Rajapakse, "Microgrids research: A review of experimental microgrids and test systems," *Renewable and Sustainable Energy Reviews*, vol. 15, no. 1, pp. 186–202, 2011.
22. P. Nguyen, W. Kling, and P. Ribeiro, "Smart power router: A flexible agent-based converter interface in active distribution networks," *IEEE Transactions on Smart Grid*, vol. 2, no. 3, pp. 487–495, 2011.
23. I. Mitra, T. Degner, and M. Braun, "Distributed generation and microgrids for small island electrification in developing countries: a review," *Solar Energy Society of India*, vol. 18, no. 1, pp. 6–20, 2008.
24. I. Araki, M. Tatsunokuchi, H. Nakahara, and T. Tomita, "Bifacial {PV} system in aichi airport-site demonstrative research plant for new energy power generation," *Solar Energy Materials and Solar Cells*, vol. 93, no. 6–7, pp. 911-916, 2009.
25. S. Morozumi, H. Nakama, and N. Inoue, "Demonstration projects for grid-connection issues in Japan," *e & i Elektrotechnik und Informationstechnik*, vol. 125, no. 12, pp. 426–431, 2008.
26. H. Hatta and H. Kobayashi, "A study of centralized voltage control method for distribution system with distributed generation," in *19th International Conference on Electricity Distribution*, Vienna, Austria, 2007, pp. 1–4.
27. M. Meiqin *et al.*, "Testbed for microgrid with multi-energy generators," in *Canadian Conference on Electrical and Computer Engineering* (CCECE), Niagara Falls, Canada, 2008, pp. 637-640.
28. R. Ray, D. Chatterjee, and S. Goswami, "Reduction of voltage harmonics using optimisation-based combined approach," *IET Power Electronics*, vol. 3, no. 3, pp. 334–344, 2010.
29. F. Huerta, J. K. Gruber, M. Prodanovic, and P. Matatagui, "Power-hardware-in-the-loop test beds: evaluation tools for grid integration of distributed energy resources," *IEEE Industry Applications Magazine*, vol. 22, no. 2, pp. 18–26, 2016.
30. S. Rajakaruna and S. Islam, "Building a state of the art laboratory for teaching and research in renewable electric energy systems and microgrids," in *IEEE Power and Energy Society General Meeting*, San Diego, USA, 2011, pp. 1–6.
31. D. Mah, P. Hills, V. Li, and R. Balme, *Smart Grid Applications and Developments, 1st* ed. London, UK: Springer, 2014.
32. T. Kerekes, M. Liserre, R. Teodorescu, C. Klumpner, and M. Sumner, "Evaluation of three-phase transformerless photovoltaic inverter topologies," *IEEE Transactions on Power Electronics*, vol. 24, no. 9, pp. 2202–2211, 2009.
33. T. Schütze, G. Borghoff, M. Wissen, and A. Höhn, *Defining the future of IGBT high-power modules* [Online]. Available: http://electronicsmaker.com/*defining-the-future-of-igbt-high-power-modules*. Accessed on: Mar. 15, 2016.
34. A. Nabae, I. Takahashi, and H. Akagi, "A new neutral-point-clamped pwm inverter," *IEEE Transactions on Industry Applications*, vol. IA-17, no. 5, pp. 518–523, 1981.
35. F. Z. Peng, "Z-source inverter," *IEEE Transactions on Industry Applications*, vol. 39, no. 2, pp. 504–510, 2003.
36. F. Peng, X. Yuan, X. Fang, and Z. Qian, "Z-source inverter for adjustable speed drives," *IEEE Power Electronics Letters*, vol. 99, no. 2, pp. 33–35, 2003.
37. M. Hanif, M. Basu, and K. Gaughan, "Understanding the operation of a z-source inverter for photovoltaic application with a design example," *IET Power Electronics*, vol. 4, no. 3, pp. 278–287, 2011.
38. L. Yang, D. Qiu, B. Zhang, and G. Zhang, "High-performance quasi-z-source inverter with low capacitor voltage stress and small inductance," *IET Power Electronics*, vol. 8, no. 6, pp. 1061–1067, 2015.
39. J. Khajesalehi, K. Sheshyekani, M. Hamzeh, and E. Afjei, "High-performance hybrid photovoltaic -battery system based on quasi-z-source inverter: application in microgrids," *IET Generation, Transmission & Distribution*, vol. 9, no. 10, pp. 895–902, 2015.
40. M. K. Nguyen, Y. C. Lim, and S. J. Park, "A comparison between single-phase quasi- z -source and quasi-switched boost inverters," *IEEE Transactions on Industrial Electronics*, vol. 62, no. 10, pp. 6336–6344, 2015.
41. Analog Devices, Inc., *ADSP-21369 EZ-KIT Lite Evaluation System Manual, 2nd* ed. Norwood, Massachusetts, USA: Analog Devices, 2012.
42. Institute of Electrical and Electronics Engineers (IEEE), *IEEE draft standard profile for use of IEEE 1588 precision time protocol in power system applications*, IEEE Standard PC37.238/D6, 2014.
43. International Electrotechnical Commission (IEC), *Communication networks and systems for power utility*

automation - Part 1: Introduction and overview, Standard IEC-61850-1:2013, 2013.
44. J. Restrepo, J. Aller, J. Viola, A. Bueno, and T. G. Habetler, "Optimum space vector computation technique for direct power control," *IEEE Transactions on Power Electronics*, vol. 24, no. 6, pp. 1637–1645, 2009.
45. M. Aredes, H. Akagi, E. Watanabe, E. Vergara, and L. Encarnacao, "Comparisons between the p–q and p–q–r theories in three-phase four-wire systems," *IEEE Transactions on Power Electronics*, vol. 24, no. 4, pp. 924–933, 2009.
46. S. Pekarek, O. Wasynczuk, and H. Hegner, "An efficient and accurate model for the simulation and analysis of synchronous machine/converter systems," *IEEE Transactions on Energy Conversion*, vol. 13, no. 1, pp. 42–48, 1998.
47. J. M. Aller, *Máquinas eléctricas rotativas: Introducción a la teoría general, 1st* ed. Caracas, Venezuela: Equinoccio, 2006.
48. P. Krause, O. Wasynczuk, and S. Pekarek, "Synchronous Machines," in *Electromechanical Motion Devices, 2nd* ed. Piscataway, New Jersey, USA: Wiley / IEEE Press, 2012, pp. 287–343.
49. X. Tan, Q. Li, and H. Wang, "Advances and trends of energy storage technology in microgrid," *International Journal of Electrical Power & Energy Systems*, vol. 44, no. 1, pp. 179-191, 2013.
50. S. Piller, M. Perrin, and A. Jossen, "Methods for state-of-charge determination and their applications," *Journal of Power Sources*, vol. 96, no. 1, pp. 113-120, 2001.
51. G. Spagnuolo *et al.*, "Control of photovoltaic arrays: Dynamical reconfiguration for fighting mismatched conditions and meeting load requests," *IEEE Industrial Electronics Magazine*, vol. 9, no. 1, pp. 62–76, 2015.
52. N. Femia, G. Petrone, G. Spagnuolo, and M. Vitelli, *Power electronics and control techniques for maximum energy harvesting in photovoltaic systems, 1st* ed. Boca Raton, Florida, USA: CRC Press, 2012.
53. G. Petrone, G. Spagnuolo, and M. Vitelli, "Analytical model of mismatched photovoltaic fields by means of lambert w-function," *Solar Energy Materials and Solar Cells*, vol. 91, no. 18, pp. 1652-1657, 2007.
54. M. Orozco, J. Ramírez, G. Spagnuolo, and C. Ramos, "A technique for mismatched {PV} array simulation," *Renewable Energy*, vol. 55, pp. 417-427, 2013.
55. J. F. Manwell, J. G. McGowan, and A. L. Rogers, *Wind energy explained: theory, design and application, 3rd* ed. West Sussex, UK: John Wiley & Sons, 2010.
56. S. Heier, *Grid Integration of Wind Energy: Onshore and Offshore Conversion Systems, 3rd* ed. West Sussex, UK: John Wiley & Sons, 2014.
57. R. Saiju, G. Arnold, and S. Heier, "Voltage dips compensation by wind farm(s) equipped with power converters as decoupling element," in *European Conference on Power Electronics and Applications*, Dresden, Germany, 2005, pp. 1–9.
58. J. Doke, *Example files for "programming with MATLAB" webinar*, 2013. [Online]. Available: http://www.mathworks.com/matlabcentral/fileexchange/43908-example-files-for--programming-with-matlab--webinar. Accessed on: Feb. 11, 2016.
59. A. Bidram and A. Davoudi, "Hierarchical structure of microgrids control system," *IEEE Transactions on Smart Grid*, vol. 3, no. 4, pp. 1963-1976, 2012.
60. J. C. Vasquez, J. M. Guerrero, M. Savaghebi, J. Eloy, and R. Teodorescu, "Modeling, analysis, and design of stationary-reference-frame droop-controlled parallel three-phase voltage source inverters," *IEEE Transactions on Industrial Electronics*, vol. 60, no. 4, pp. 1271–1280, 2013.
61. B. Sahan, S. V. Araújo, C. Nöding, and P. Zacharias, "Comparative evaluation of three-phase current source inverters for grid interfacing of distributed and renewable energy systems," *IEEE Transactions on Power Electronics*, vol. 26, no. 8, pp. 2304–2318, 2011.
62. B. Exposto *et al.*, "Three-phase current-source shunt active power filter with solar photovoltaic grid interface," in *IEEE International Conference on Industrial Technology* (ICIT), Seville, Spain, 2015, pp. 1211–1215.
63. H. Han *et al.*, "Review of power sharing control strategies for islanding operation of ac microgrids," *IEEE Transactions on Smart Grid*, vol. 7, no. 1, pp. 200–215, 2016.
64. J. M. Guerrero, L. Hang, and J. Uceda, "Control of distributed uninterruptible power supply systems," *IEEE Transactions on Industrial Electronics*, vol. 55, no. 8, pp. 2845–2859, 2008.
65. T. Vandoorn, J. D. Kooning, B. Meersman, and L. Vandevelde, "Review of primary control strategies for islanded microgrids with power-electronic interfaces," *Renewable and Sustainable Energy Reviews*, vol. 19, pp. 613–628, 2013.
66. L. E. Luna, H. Torres, and F. A. Pavas, "Spinning reserve analysis in a microgrid," *Dyna*, vol. 82, no. 192, pp. 85–93, 2015.
67. A. Mehrizi and R. Iravani, "Potential-function based control of a microgrid in islanded and grid-connected modes," *IEEE Transactions on Power Systems*, vol. 25, no. 4, pp. 1883–1891, 2010.
68. A. Bidram, A. Davoudi, F. L. Lewis, and Z. Qu, "Secondary control of microgrids based on distributed cooperative control of multi-agent systems," *IET Generation, Transmission & Distribution*, vol. 7, no. 8, pp. 822–831, 2013.
69. M. Ding, Y. Y. Zhang, M. Q. Mao, W. Yang, and X. P. Liu, "Operation optimization for microgrids under centralized control," in *2nd IEEE International Symposium on Power Electronics for Distributed Generation Systems* (PEDG), Hefei, China, 2010, pp. 984–987.
70. L. Meng, J. M. Guerrero, J. C. Vasquez, F. Tang, and M. Savaghebi, "Tertiary control for optimal unbalance compensation in islanded microgrids," in *11th International Multi-Conference on Systems, Signals & Devices* (SSD), Barcelona, Spain, 2014, pp. 1–6.